Eur. Phys. J. D **64**, 297–301 (2011)
DOI: 10.1140/epjd/e2011-20352-4

THE EUROPEAN PHYSICAL JOURNAL D

Regular Article

Energy-loss straggling study of proton and alpha-particle beams incident onto ZrO_2 and Al_2O_3 films

M. Behar[1], R.C. Fadanelli[1], I. Abril[2,a], R. Garcia-Molina[3], and L.C.C. Nagamine[4]

[1] Instituto de Fisica, Universidade Federal do Rio Grande do Sul, Porto Alegre, 91501-970, Brazil
[2] Departament de Física Aplicada, Universitat d'Alacant, 03080 Alacant, Spain
[3] Departamento de Física – Centro de Investigación en Óptica y Nanofísica, Universidad de Murcia, 30100 Murcia, Spain
[4] Instituto de Física, Universidade de São Paulo, C.P. 66318, 05315-970 São Paulo, Brazil

Received 14 June 2011
Published online 11 October 2011 –

Abstract. The energy-loss straggling of zirconia (ZrO_2) and alumina (Al_2O_3) has been experimentally determined for proton and alpha-particle beams mainly by means of the Rutherford backscattering technique and in some few cases using the transmission method. The incident energies of the projectiles covers a wide range, from 200 keV up to 2000 keV for H^+ and from 200 keV up to 4000 keV for He^+ in zirconia films. In the case of alumina films the studied energy range was 100 keV–3000 keV for H^+ and 100 keV–6000 keV for He^+. Our experimental results compare very well with theoretical calculations based on the dielectric formalism and a suitable description of the electronic excitation spectrum of ZrO_2 and Al_2O_3 films through their energy-loss function.

1 Introduction

Zirconia and alumina are two large-band-gap insulators with many technological applications due to their excellent mechanical, thermal and optical properties. In particular, zirconia has a wide range of industrial applications including its uses in ceramic engineering, as catalytic support medium, or as bone prosthetics in dentistry and orthopaedy [1] and the references therein; it has also been proposed due to its high dielectric constant, together with hafnia (HfO_2), as a gate dielectric material in metal-oxide semiconductor devices [2]. Moreover, zirconia is one of the most radiation-resistant ceramics which makes it important in the nuclear industry. On the other hand, alumina is a useful material for a variety of purposes with potential applications in optics and optoelectronics [3], and it is a common choice as a protective or supporting film for waveguides, solid state lasers, and other devices [4]. Therefore, due to their technological importance, ZrO_2 and Al_2O_3 are materials commonly found in ion beam analysis experiments, where a detailed knowledge of their energy-loss distribution and energy-loss straggling are indispensable.

A great effort has been devoted to obtain accurate experimental data of the stopping power of ZrO_2 and Al_2O_3 films for energetic ions [5–12]. However, up to now, there are not measurements of the energy-loss straggling for proton and alpha-particle beams in zirconia and in alumina. This lack of experimental data can be attributed to the great complexity to perform precise energy-loss straggling measurements in compounds and insulators targets, such as in the oxides analyzed here. The main experimental difficulties lie in the preparation of homogeneous and smooth films, since inhomogeneities in the irradiated target may contribute into the measured energy loss fluctuations [13]. Besides, fluctuations of the projectile charge-state, and spatial correlation effects mean an additional problem. On the other hand, from the point of view of particle-matter interaction it is essential to know the energy-loss straggling as well as the stopping power, nevertheless theoretical calculations of the straggling are quite limited [14–21] as compared with the stopping power literature.

In this work, we present, for the first time, experimental data of the energy-loss straggling of proton and alpha-particle beams interacting with ZrO_2 and Al_2O_3 films in a broad projectile energy range. These measurements have been done using mainly the Rutherford backscattering technique for projectile energies in the range of hundreds of keV up to several MeV, together with a few measurements using the transmission method, which include the region around the maximum stopping power. Theoretical calculations of the energy-loss straggling have been performed in the frame of the dielectric formalism (first Born approximation) with a suitable description of the ZrO_2 and Al_2O_3 energy loss functions (ELF), provided by the MELF-GOS method [18,22]. The agreement between the experimental data and the theoretical results is very good.

2 Experimental method

The ZrO_2 as well as the Al_2O_3 films were prepared by the radio frequency magnetron sputtering technique using

[a] e-mail: ias@ua.es

commercial targets and O_2/Ar mixture as a sputtering gas. The ZrO_2 target has a nominal purity of 99.9% (with a Hf impurity content of 5% wt); ZrO_2 films of thicknesses $t = 13$, 37, 54, 68, 95, 145 and 190 nm were deposited onto Si (100) substrates by varying the deposition time. In the case of the Al_2O_3 films the same procedure was followed; the target purity was of 99.99% and films of thicknesses $t = 14$, 27, 41, 54, 100 and 150 nm were deposited on a polished carbon substrate. Checking of thickness and roughness of both kinds of films were done by using the X-ray reflectivity scan (XRR) technique [23] together with the software WinGixa from Philips. The typical error in the film thicknesses was of ∼4%. The roughness of the films was estimated to be around 6% of their thickness.

The incident energies of the projectiles cover a wide range. For ZrO_2 it was from 200 keV up to 2000 keV for H^+, and from 200 keV up to 4000 keV for He^+. For the Al_2O_3 films, the energy range interval was from 100 keV up to 3000 keV for H^+ and from 100 keV up to 6000 keV for He^+. The total energy resolution of the system (FWHM) was 6 keV for H^+ and 10 keV for He^+, respectively. The ion beams were provided by the 500 kV ion implanter and the 3 MV Tandetron accelerator of the Instituto de Fisica of the Universidade do Rio Grande do Sul, Brazil.

For each incident ion energy, we have used the appropriate film and three spectra were recorded at 0°, 30° and 45° between the normal of the sample and the incident ion beam in order to have better precision in our final results. In Figure 1a we show the He, 1.2 MeV RBS spectrum, obtained with the 95 nm ZrO_2 film taken at 30° of incidence. In all the cases a Si(Li) particle-detector, with constant efficiency for the analyzed energy range, was situated at 170° with respect to the ion-beam direction. As can be observed, this spectrum shows the existence of the Hf signal, which is due to the presence of this element in the sputter target used in the present experiment. Figure 1b shows a detail of the Al signal corresponding to the RBS spectrum of 3 MeV He incident at 30° on the 150 nm Al_2O_3 film. The stoichiometry of the films was checked by using the Rutherford backscattering technique (RBS). The results show that they are, within 3%, in the right proportion.

We want to stress that the analysis of the straggling data for each element was done on the Zr signal for the ZrO_2 case, and on Al signal when we deal with the Al_2O_3 films. We chose this procedure because in each case the heavier elements have a larger cross section as compared with the lighter ones. The straggling was obtained by fitting the measured spectra; in reference [20] details on sample preparation, experimental and fitting procedure are explained.

In addition, it is worth to mention that the lowest energy straggling data for He in Al_2O_3 (from 30 up to 60 keV) was measured by Eckardt and Lantschner [24] by using the transmission technique with self-supported 12 nm thin foils. The He beam was provided by an rf source with a further electrostatic acceleration stage. The energy analysis was performed by an electrostatic device

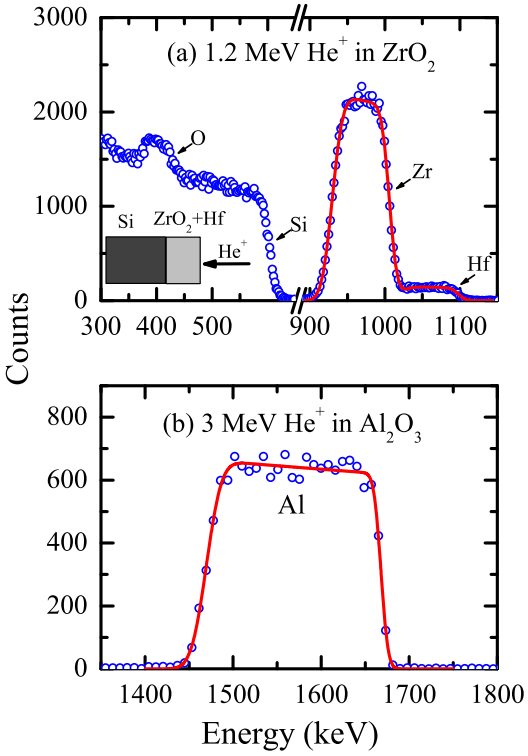

Fig. 1. (Color online) (a) Rutherford backscattering spectrum corresponding to a 1.2 MeV alpha-particle beam incident on a 95 nm-thick ZrO_2 film with an angle of incidente 30°. (b) Detail of the Al signal corresponding to the Rutherford backscattering spectrum of a 3 MeV alpha-particle beam incident at an angle 30° on a 150 nm-thick Al_2O_3 film. The line denotes the fitting to the experimental results (symbols), which was used to extract the energy-loss straggling. The Si(Li) particle detector is located at 170° with respect to the incident beam direction.

with an energy resolution (FWHM) of 0.3%. Spectra were recorded by a multichannel scaler with channels switched synchronously with the energy analyzer plate potential. Details of the use of this technique can be found also in reference [20].

3 Theoretical calculations

Bohr [25] was the first to evaluate the electronic energy-loss straggling for swift (but non-relativistic) particles penetrating a thin target, assuming that all the target electrons are free. The Bohr straggling is given by

$$\Omega^2_{\text{Bohr}} = 4\pi Z_1^2 Z_2 e^2 N, \quad (1)$$

where Z_1 and Z_2 are the atomic numbers of the projectile and the target, respectively, e is the elemental charge, and N is the density of target atoms; for ZrO_2 (Al_2O_3) films $Z_2 = 56$ (50) and $N = 2.74 \times 10^{-2}$ molec/Å^3 (2.34×10^{-2} molec/Å^3). Since the Bohr straggling applies for free-Coulomb scattering between a penetrating point charge and a random assembly of free target electrons, it is a

common standard reference at the high projectile velocity limit.

When the irradiated target is a compound, as in the case of ZrO_2 and Al_2O_3, aggregation (physical state and chemical bonding) effects must be considered, and a detailed description of the involved energy-loss processes is necessary to calculate the energy-loss straggling in a broad projectile energy range. The dielectric formalism [26], which is based in the first order Born approximation, provides the energy-loss straggling of a projectile (with atomic number Z_1 and mass M_1) travelling with a kinetic energy E through a target, characterized by its dielectric function ε, by the following expression [20]:

$$\Omega^2 = \frac{e^2\hbar M_1}{\pi E}\sum_{q=0}^{Z_1}\phi_q\int_0^{\infty}dk\frac{\rho_q^2(k)}{k} \times \int_0^{k\sqrt{2E/M_1}}d\omega\,\omega^2\mathrm{Im}\left[\frac{-1}{\varepsilon(k,\omega)}\right], \quad (2)$$

where $\hbar\omega$ and $\hbar k$ are, respectively, the energy and momentum transferred to the target in an inelastic process, and $\mathrm{Im}[-1/\varepsilon(k,\omega)]$ is the energy loss function (ELF) of the material. This equation also accounts for the processes of electron capture and loss by the projectile in its path through the solid, which implies that its charge state q can vary in the range $0 \leq q \leq Z_1$ according to a given probability ϕ_q.

As the charge equilibrium is reached quasi instantaneously after the projectile penetrates into the solid, we assume that ϕ_q represents the charge-state fraction at equilibrium, which depends on the target nature, the projectile and its energy. The energy dependence of ϕ_q is obtained by the parameterization to experimental data given by [27]. $\rho_q(k)$ is the Fourier transform of the projectile charge-density for the charge-state q, which is described by the statistical Brandt-Kitagawa model [28,29]. The only target-depending magnitude in equation (2) is the energy-loss function, $\mathrm{Im}[-1/\varepsilon(k,\omega)]$, which fully characterizes the electronic excitation spectrum of the target and accounts for its response to external perturbations. To obtain reliable values of the energy-loss straggling a proper description of the target ELF is essential, in such a manner that it provides a realistic information of the target electronic excitations and ionizations.

We describe the energy-loss function of ZrO_2 and Al_2O_3 through the MELF-GOS method (Mermin energy loss function-generalized oscillator strength) [18,22], which accounts for the loosely bound electrons of the target using a linear combination of Mermin-type ELF (MELF), fitted to the experimental ELF at the optical limit ($k = 0$). The inner-shell electron excitations are described by the generalized oscillator strength (GOS) in the hydrogenic approach. Also, the MELF-GOS method demands that the fitting ELF satisfy the f-sum rule [30]. The advantage of this methodology lies on a realistic description of the experimental optical energy-loss spectrum, the inclusion of the finite plasmon lifetime, and an analytical extension of the ELF to finite momentum transfers without ad hoc suppositions [31].

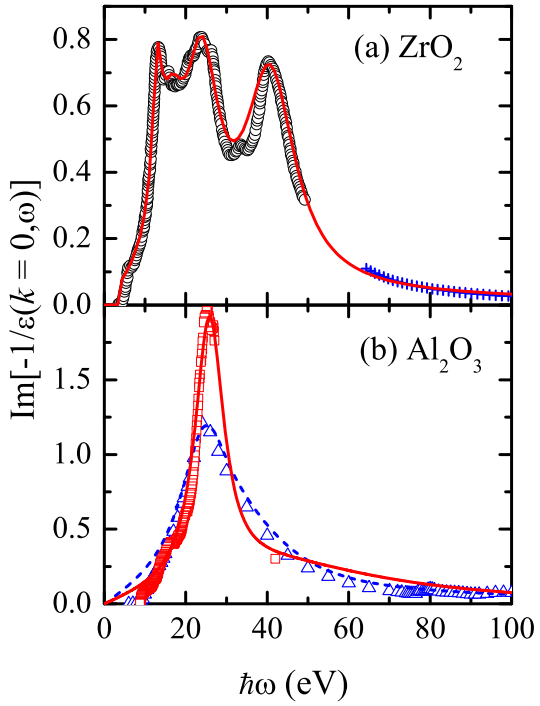

Fig. 2. (Color online) (a) Optical energy-loss function of ZrO_2; symbols correspond to experimental values from [32] (○) and from [33] (+) in two different regions, whereas line represents the fitting from the MELF-GOS model. (b) Optical energy-loss function of Al_2O_3 with symbols representing two different sets of experimental data covering the same region: Δ [34] and □ [35]. Lines represent the corresponding fitting curves obtained by the MELF-GOS model.

In Figure 2a we show the experimental optical ELF of ZrO_2 [32] (black round symbols) together with the data obtained from X-rays experiments [33] (blue crosses), which have been fitted by the MELF-GOS method (line) with the parameters described in reference [6], and where the electrons from the K-shell of O, as well as the K- and L-shells of Zr are treated as inner electrons. On the other hand, there are two set of experimental data [34,35] for the ELF at the optical limit ($k = 0$) of Al_2O_3, which are depicted by symbols in Figure 2b, where the lines represent the fitting through the MELF-GOS method to each set of experimental data; for the Al_2O_3 target we consider as inner-electrons the K-shells of Al and O.

4 Results and discussion

The experimental energy-loss straggling of proton and alpha-particle beams in ZrO_2 and Al_2O_3 films is presented in Figures 3 and 4, respectively, as a function of the projectile energy. These experimental data have been corrected for the effects of foil roughness [36] and cover a wide range of projectile energies, as mentioned in Section 2, which

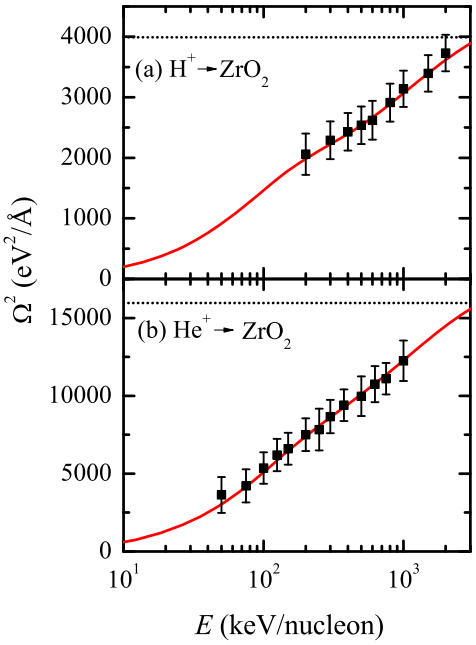

Fig. 3. (Color online) Experimental energy-loss straggling of ZrO_2 for (a) proton and (b) alpha-particle beams (symbols with error bars). The straggling calculated by equation (2) is depicted by a solid line. For comparison purposes, the Bohr straggling is shown by a dotted horizontal line.

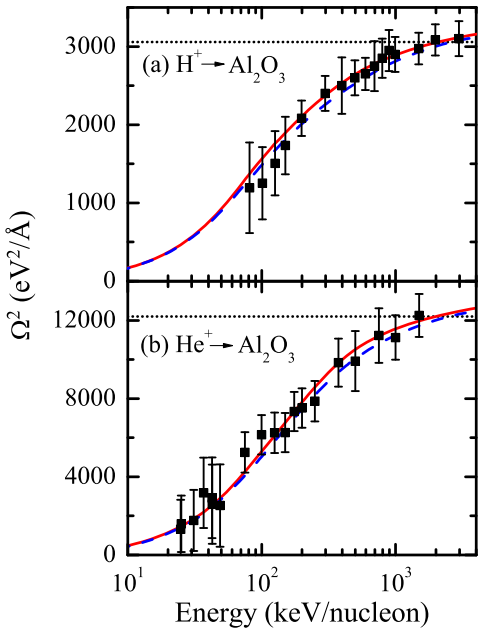

Fig. 4. (Color online) Experimental energy-loss straggling of Al_2O_3 for (a) proton and (b) alpha-particle beams (symbols with error bars). The lowest energy data (30 to 60 keV) for He ions have been kindly provided by Eckardt and Lantschner [24], who used the transmission technique. The straggling calculated by equation (2) when using two different sets of optical ELF are depicted by solid and dashed lines derived from corresponding to the experimental ELF data of references [35] and [34] respectively, as shown in Figure 2b. The Bohr straggling is shown by a dotted horizontal line.

includes in both cases the energies corresponding to the maximum value of the stopping power.

Lines in Figures 3 and 4 represent the calculated energy-loss straggling in ZrO_2 and Al_2O_3, respectively, through equation (2), by using the MELF-GOS method to describe the ELF of each target. In the case of Al_2O_3, where there are two different sets of experimental optical-ELF data [34,35], we have evaluated the energy-loss straggling in both cases (dashed and solid lines in Fig. 4). Despite the difference between the two ELF for Al_2O_3 used in our calculations (shown in Fig. 2), no significant discrepancies appear in the calculated Ω^2 with the maximum difference being ≈5%. This similitude of results is mainly due to two facts. In the first place, the particular details of the ELF at low transferred energies scarcely affect the calculated energy-loss straggling. In the second place, in both fittings to the optical experimental data the ELF satisfies sum rules [30], which are physical constraints related directly to the atomic properties of the target; besides, the inner-shell electron excitation spectrum is the same in both cases. In addition, the ω^2 term appearing in the calculation of Ω^2, equation (2), gives more weight to the ELF at large energy transfer, and both experimental ELF [34,35] are very similar for $\hbar\omega \geq 100$ eV.

The comparison of both, experimental and calculated energy-loss straggling of ZrO_2 and Al_2O_3 films for proton and alpha-particle beams show a very good agreement, for all the range of energies considered in this work.

5 Conclusions

The experimental energy-loss straggling of ZrO_2 and Al_2O_3 for proton and alpha-particle beams is presented for the first time. These results will be useful for a better characterization of the energy loss of swift H^+ and He^+ beams in zirconia and alumina films, which are two materials with important applications. The projectile energies cover a wide range, which includes the energy corresponding to the maximum stopping power. Comparison with the results derived from a theoretical model based on the dielectric formalism together with a realistic description of the energy loss spectrum of ZrO_2 and Al_2O_3 show an excellent agreement in the whole energy range of measurements.

We acknowledge the authors of reference [24] for providing us their unpublished results. This work has been financially supported by the Brazilian Conselho Nacional de Pesquisas (CNPq) and the Spanish Ministerio de Ciencia e Innovación (Project FIS2010-17225).

References

1. G. Fadda, L. Colombo, G. Zanzotto, Phys. Rev. B **79**, 214102 (2009)
2. R. Puthenkovilakam, E.A. Carter, J.P. Chang, Phys. Rev. B **69**, 155329 (2004)

3. A.J. Dan'ko, S.V. Nizhankovskiy, V.M. Puzikov, L.A. Grin', N.S. Sideinikova, G.T. Adonkin, V.N. Kanishchev, Crystall. Rep. **53**, 1272 (2008)
4. D. Yan, J. He, X. Li, L. Jianxin, Z. Huili Ding, Surf. Coat. Technol. **141**, 1 (2001)
5. Y. Zhang, W.J. Weber, Nucl. Instr. Methods B **267**, 1705 (2009)
6. M. Behar, C.D. Denton, R.C. Fadanelli, I. Abril, E.D. Cantero, R. Garcia-Molina, L.C.C. Nagamine, Eur. Phys. J. D **59**, 209 (2010)
7. P. Bauer, W. Rossler, P. Mertens, Nucl. Instr. Methods B **69**, 46 (1992)
8. D.C. Turner, N.F. Mangelson, L.B. Rees, Nucl. Instr. Methods B **103**, 28 (1995)
9. K. Eder, D. Semrad, P. Bauer, R. Golser, P. Maier-Komor, F. Aumayr, M. Peñalba, A. Arnau, J.M. Ugalde, P.M. Echenique, Phys. Rev. Lett. **79**, 4112 (1997)
10. D.C. Santry, R.D. Werner, Nucl. Instr. Methods B **14**, 169 (1986)
11. P. Bauer, R. Golser, D. Semrad, P. Maier-Komor, F. Aumayr, A. Arnau, Nucl. Instr. Methods B **136-138**, 103 (1998)
12. C. Pascual-Izarra, M. Bianconi, N.P. Barradas, A. Climent-Font, G. García, J. Gonzalo, C.N. Afonso, Nucl. Instr. Methods B **219-220**, 268 (2004)
13. J.C. Eckardt, G.H. Lantschner, Nucl. Instr. Methods B **175-177**, 93 (2001)
14. W.K. Chu, Phys. Rev. A **13**, 2057 (1976)
15. Y. Kido, T. Koshikawa, Phys. Rev. A **44**, 1759 (1991)
16. Q. Yang, D.J. O'Connor, Z. Wang, Nucl. Instr. Methods B **61**, 149 (1991)
17. I. Abril, R. Garcia-Molina, N.R. Arista, C.F. Sanz-Navarro, Nucl. Instr. Methods B **190**, 89 (2002)
18. S. Heredia-Avalos, R. Garcia-Molina, J.M. Fernández-Varea, I. Abril, Phys. Rev. A **72**, 052902 (2005)
19. C.C. Montanari, J.E. Miraglia, S. Heredia-Avalos, R. Garcia-Molina, I. Abril, Phys. Rev. A **75**, 022903 (2007)
20. I. Abril, M. Behar, R. Garcia-Molina, R.C. Fadanelli, L.C.C.M. Nagamine, P.L. Grande, L. Schunemann, C.D. Denton, N.R. Arista, E.B. Saitovitch, Eur. Phys. J. D **54**, 65 (2009)
21. P. Sigmund, A. Schinner, Eur. Phys. J. D **58**, 105 (2010)
22. I. Abril, R. Garcia-Molina, C.D. Denton, J.F. Peréz-Pérez, N.R. Arista, Phys. Rev. A **58**, 357 (1998)
23. W. Wu, W.E. Wallace, E.K. Lin, G.W. Lynn, C.J. Glinka, E.T. Ryan, H.-M. Ho, J. Appl. Phys. **87**, 1193 (2000)
24. J.C. Eckardt, G.H. Lantschner, unpublished data, private communication
25. N. Bohr, Phil. Mag. **30**, 581 (1915)
26. J. Lindhard, Kong. Dans. Videns. Selsk. **28** (1954)
27. G. Schiwietz, P.L. Grande, Nucl. Instr. Methods B **175-177**, 125 (2001)
28. W. Brandt, M. Kitagawa, Phys. Rev. B **25**, 5631 (1982)
29. Corrections to the BK model appear in W. Brandt, Nucl. Instrum. Methods Phys. Res. **194**, 13 (1982)
30. S. Tanuma, C.J. Powell, D.R. Penn, J. Electr. Spectrosc. Relat. Phenom. **62**, 95 (1993)
31. R. Garcia-Molina, I. Abril, I. Kyriakou, D. Emfietzoglou, in *Radiation Damage in Biomolecular Systems*, edited by M. Fuss, G. García (Canopus Academic, London)
32. J. Frandon, B. Rousseau, F. Pradal, Phys. Stat. Sol. B **98**, 379 (1980)
33. B.L. Henke, E.M. Gullikson, J.C. Davis, At. Data Nucl. Data Tables **54**, 181 (1993)
34. H.-J. Hagemann, E. Gudat, C. Kunz, J. Opt. Soc. Am. **65**, 742 (1975)
35. R.H. French, H. Mullejans, D.J. Jones, J. Am. Ceram. Soc. **81**, 2549 (1998)
36. F. Besenbacher, J.V. Andersen, E. Bonderup, Nucl. Instrum. Methods **168**, 1 (1980)